A Simple Solution Route to Single-Crystalline Sb_2O_3 Nanowires with Rectangular Cross Sections

Zhengtao Deng,[†,§] Fangqiong Tang,*[,†] Dong Chen,[†] Xianwei Meng,[†] Li Cao,[‡] and Bingsuo Zou[‡]

Technical Institute of Physics and Chemistry, Chinese Academy of Sciences, Beijing 100080, China, Institute of Physics, Chinese Academy of Sciences, Beijing 100080, China, and Graduate University of Chinese Academy of Sciences, Beijing 100080, China

Received: June 15, 2006; In Final Form: July 10, 2006

We report a simple solution route to large-scale synthesis of uniform, single-crystalline, and well-faceted orthorhombic antimony trioxide (Sb_2O_3) nanowires with rectangular cross sections by direct air oxidation of bulk metal antimony (Sb) in a mixed solution made of ethylenediamine (EDA) and deionized water (DIW). The as-synthesized products were analyzed by range of methods, such as XRD, SEM, EDX, TEM, SAED, HRTEM, FTIR, Raman, UV−vis absorption, and photoluminescence (PL) spectra. The as-synthesized Sb_2O_3 nanowires with rectangular cross sections are usually hundreds of micrometers in length, typically 80−100 nm in width, and 60−80 nm in thickness. The novel room temperature photoluminescence properties of Sb_2O_3 nanowires with rectangular cross sections displayed a significant UV luminescence with a strong emission band at 374 nm, which was reported for the first time, indicating the as-synthesized products with an optical band gap $E_g = 3.3$ eV. It is expected that as-synthesized Sb_2O_3 nanowires would be a new member of functional materials and used in the manufacture of advanced nanodevices.

1. Introduction

In recent years, thanks to the blooming development of nanoscience and nanotechnology, one-dimensional (1D) metal oxide semiconductor nanowires, such as ZnO, In_2O_3, Ga_2O_3, and SnO_2, have attracted considerable interest for scientific research because of their remarkable electronic, optical, catalytic, and mechanical properties, which are different from those of the bulk materials, and these nanomaterials may eventually lead to technological applications in the manufacture of optoelectronic nanodevices.[1−10]

Antimony trioxide (Sb_2O_3) is an important member of V−VI main group compounds and has been widely used in industry in the past century: (1) as a fire retardant in membranes in the plastics industry and as enclosures of electric devices such as PVC, PP, PE, PS, ABS, et al.;[11−13] (2) as filling, covering agents, and retardants for rubber, ceramics, enamels, fabrics, and fiber products; and (3) as a catalytic agent in organic synthesis, especially in combination with vanadium, uranium, molybdenum oxide, or iron oxide for propane ammoxidation and propene oxidation and ammoxidation.[14−17] Similar to the other well-studied metal oxide semiconductors, antimony trioxide (Sb_2O_3) is also expected to be an interesting semiconducting material exhibiting unique optical and optoelectronic properties. However, less attention has been paid to the emission properties of Sb_2O_3 since it is an indirect-gap semiconductor with low emission efficiency. To the best of our knowledge, little knowledge has been obtained for the optical properties of Sb_2O_3, especially for their photoluminescence properties.

Several synthesis methods for 1D Sb_2O_3 nanostructures have been reported in the literature. For example, Sb_2O_3 nanorods have already been prepared by using a microemulsion method,[18] by hydrothermal conditions,[19] by using carbon nanotubes as the template,[20] or by a vapor-solid route.[21] Sb_2O_3 nanowires and nanotubes have been prepared by a surfactant-assisted solvothermal approach.[22] More recently, Sendor et al. reported that Sb_2O_3 nanobelts could be obtained by a solid-to-nanostructure transformation process, in which the size of the obtained nanobelts ranged up to 15 μm in length with diameters between 8 and 50 nm.[23] Nevertheless, these 1D Sb_2O_3 nanostructures are neither uniform nor well crystallized, thus uniform single-crystalline 1D Sb_2O_3 nanostructures with the desired quality for use in nanodevices is still a great challenge. What is more, as recent research has suggested, in addition to size and dimension, the cross-section also has a shape effect on the properties of nanomaterials,[24] but only a limited number of one-dimensional metal oxide semiconductors with rectangular cross-sections have been reported such as ZnO[25,26] and VO_2.[27]

In this paper, we report a simple solution route for the large-scale synthesis of uniform, single-crystalline, well-faceted Sb_2O_3 nanowires with rectangular cross sections by direct air oxidation of bulk metal antimony (Sb) in a mixed solution made of ethylenediamine (EDA) and deionized water (DIW), instead of the common coprecipitation of antimony salts.[18−20,22] The advantages of the present protocol are the following: (1) We have obtained highly uniform, well-crystallized single-crystalline Sb_2O_3 nanowires with rectangular cross sections, a new nanostructure of Sb_2O_3 not reported before. (2) We take bulk metal antimony (Sb) and oxygen in air as source materials, which are cheap, "green", and easy to scale-up. (3) Our preliminary data indicate that these nanowires with rectangular cross sections displayed a significant room temperature UV luminescence with an emission band at 374 nm, which was reported for the first

* Address correspondence to this author. E-mail: tangfq@mail.ipc.ac.cn. Phone: 86-10-82543521. Fax: +86-10-62554670.

† Technical Institute of Physics and Chemistry, Chinese Academy of Sciences.

‡ Institute of Physics, Chinese Academy of Sciences.

§ Graduate University of Chinese Academy of Sciences.

10.1021/jp063748y CCC: $33.50
Published on Web 08/23/2006

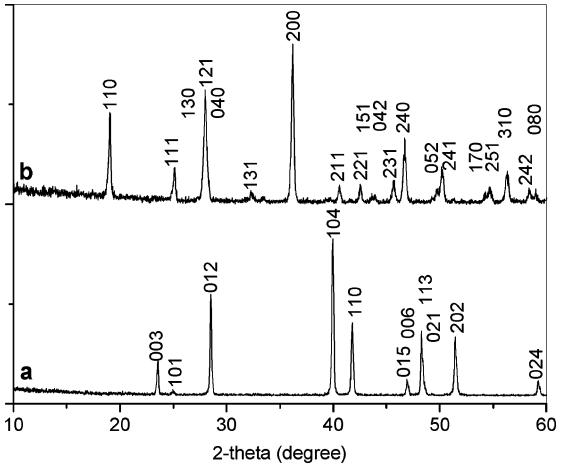

Figure 1. XRD profile of the source material (a) and the as-synthesized products (b).

time. The nanowires with rectangular cross sections are usually hundreds of micrometers in length, typically 80−100 nm in width, and 60−80 nm in thickness, and they are expected to be good candidates for further studies and applications in nanoscale technology.

2. Experimental Section

All of the chemical reagents used in this experiment were analytical grade. In a typical experiment, 120 mg of antimony (Sb) powder (<200 mesh, 99.5%), 400 mg of poly(vinylpyrrolidone) (PVP, MW 30 000), and 9 mmol of ethylenediamine (EDA), were added into 74 mL of deionized water (DIW). Then, the mixed solution was stirred at room temperature for 5 h. After the reaction, the resulting white solid products were filtered and washed with distilled water to remove residual ions in the products. The final products were then dried in air at 60 °C for 4 h before characterization.

X-ray powder diffraction (XRD) employed a Japan Regaku D/max γA X-ray diffractometer equipped with graphite monochromatized Cu KR radiation ($\lambda = 1.5418$ Å) irradiated with a scanning rate of 0.02 deg/s. Scanning electron microscopy (SEM) and energy-dispersive X-ray spectroscopic (EDX) measurement were performed on powder samples deposited on silica substrates with a Hitachi S-4300 Scanning Electron Field Emission Microscope operating at 15 kV. A JEOL JEM-200CX microscope operating at 160 kV in the bright-field mode was used for Transmission Electron Microscopy (TEM). Selected area electron diffraction (SAED) pattern and high-resolution TEM (HRTEM) were performed on a JEOL JEM-2010 electron microscope operating at 200 kV. Fourier transform infrared (FTIR) spectra were recorded with a Bio-Rad FTIR spectrometer FTS 165. Micro-Raman experiments were conducted in a Raman scattering spectrometer (LABRAM-HR, JY, Horiba), with the 514.5 nm line of an Ar^+ laser as the excitation source. Ultraviolet and visible absorption (UV−vis) spectra were recorded with a JASCO 570 spectrophotometer at room temperature. Photoluminescence (PL) spectra were measured with a PTI-C-700 fluorescence spectrometer.

3. Results and Discussion

Figure 1 shows the typical XRD patterns of the source material and the as-synthesized products. All the diffraction peaks of the source material can be readily indexed as a high pure metal Sb phase (JCPDS Card No.77-1173). In contrast, the experimental XRD profile taken from the as-synthesized products showed that all of the peaks may be indexed as the orthorhombic phase Sb_2O_3 (cell constants a =4.911 Å, b = 12.464 Å, c = 5.412 Å; JCPDS Card No. 11-0689). No peaks of metal Sb or any other phases were detected, indicating that the products are very high purity, single-phase samples. In addition, the intense and sharp diffraction peaks suggest the as-synthesized products are well crystallized. Furthermore, as seen from the XRD pattern of the as-synthesized products, the (110) and the (200) peak intensities are significantly enhanced, and the (121) and the (111) peak intensities are significantly decreased relative to bulk orthorhombic phase Sb_2O_3, indicating the preferred crystallographic orientation of the products.

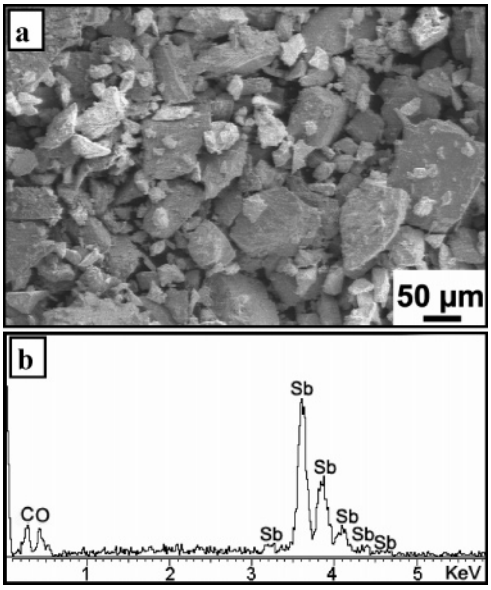

Figure 2. (a) SEM image and EDX pattern of the source material.

The morphologies of the source material and the as-synthesized products were determined with SEM. Figure 2 shows the typical SEM image and EDX pattern of the source materials metal bulk antimony, which revealed that the sizes of the irregular shaped antimony particles ranged from 10 to 100 μm. The EDX spectrum obtained from a single particle is shown in the inset of Figure 2b. Only Sb peaks are observed in this spectrum (small carbon and oxygen signal from the substrate), indicating that the source material is pure metal Sb. Typical SEM images of the products are shown in Figure 3. As can be seen, panels a and b of Figure 3 show that the products contain a large quantity of uniform wire-like materials. The lengths of the products are up to hundreds of micrometers. Figure 3c shows the high-magnification SEM image of three typical nanowires, indicating the as-synthesized nanowires are very highly uniform. Closer inspection revealed that the geometrical shape of the 1D sample appears to be that of a cuboidal morphology with a rectangular cross section; as seen from Figure 3d−f, the nanowires are about 80∼100 nm in width, and are about 60∼80 nm in thickness. To determine the composition of the nanowires, EDX was performed on individual nanowires with rectangular cross sections. Figure 3g is an EDX spectrum obtained from a single nanowire shown in the inset of Figure 3c. Only Sb and O peaks are observed in this spectrum (silicon signal from the silicon substrate), suggesting that the nanowires are composed of mainly Sb and O. Quantitative EDX analysis shows that the atom ratio of Sb/O is 39:61, close to 2:3, indicating the composition of the as-synthesized products is Sb_2O_3.

The morphologies of the as-synthesized products were further investigated by TEM as shown in Figure 4, which also shows

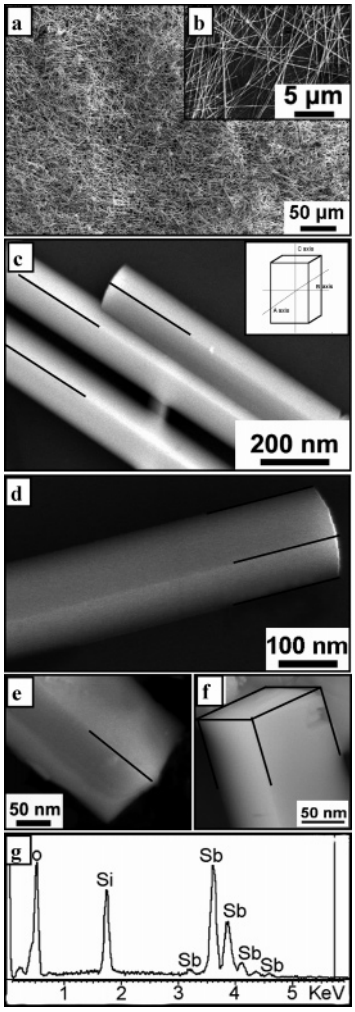

Figure 3. (a and b) Low-magnification SEM images of the products showing that the products contain a large quantity of Sb_2O_3 nanowires. (c−f) High-magnification SEM images of the nanowires showing the nanowires with rectangular cross sections. (g) EDX spectrum taken from a single nanowire giving the nanowires a possible composition of Sb_2O_3. The inset in panel c represents the orthorhombic crystal cell of the Sb_2O_3.

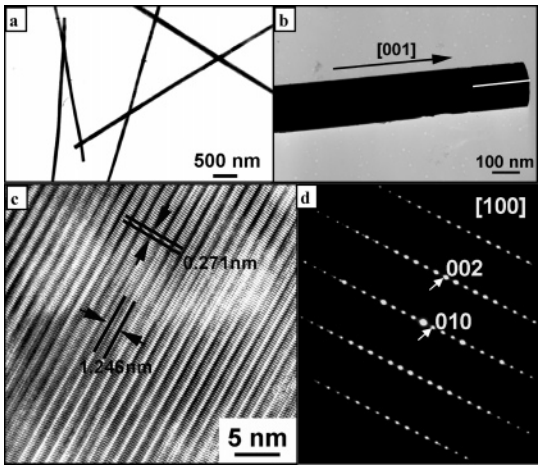

Figure 4. (a and b) Typical TEM image of Sb_2O_3 nanowires with rectangular cross sections. (c) Typical HRTEM image of a single Sb_2O_3 nanowires. (d) The corresponding SAED pattern.

the uniform Sb_2O_3 nanowires with a width of about 80−100 nm and a length up to several hundreds of micrometers. The microstructure of an individual Sb_2O_3 nanowire was further investigated in detail by HRTRM and SAED. A typical HRTEM image of a single Sb_2O_3 nanowire is shown in Figure 4c. The lattice spacings of about 1.246 and 0.271 nm correspond to (010) and (002) planes spacings of orthorhombic phase Sb_2O_3 (JCPDS Card No. 11-0689), respectively. The SAED pattern (shown in Figure 4d) taken along the [100] zone axis is a spot pattern, which reveals that the nanowire is a single crystal in nature. Both the HRTEM image and the SAED pattern demonstrate that the nanowire grows along the [001] direction indicated with an arrow in Figure 4b. In addition, Figure 4 also reveals that the nanowires with rectangular cross sections are well crystallized and free from dislocation and stacking faults.

The growth mechanism is also investigated. As shown in Figure 2a, the sizes of the irregularly shaped antimony particles ranged from 10 to 100 μm. It is well-known that the oxidation of antimony metal by naturally dissolved oxygen in water is very slow, and it usually transforms into Sb_2O_3, when antimony is oxidized in a humid environment. It is believed that in our experiments EDA possibly acted as a catalyst, thus the presence of EDA would change the microenvironment for the electrochemical reaction; therefore, the spontaneous oxidation reaction of antimony metal is accelerated drastically, and it transforms into Sb_2O_3, while oxygen is reduced in the reaction. As a result, the amount of EDA has a significant influence on the shape and shape evolution of the products. If no EDA was added, there were almost no Sb_2O_3 products obtained, because the direct oxidation of antimony metal by naturally dissolved oxygen in water is very slow, while if the amount of EDA was very large (over 15 mmol), only micrometer-scale irregularly shaped Sb_2O_3 would be obtained, possibly because the reaction rate was extremely rapid. Similar results for EDA helping to synthesize $Co(OH)_2$ nanorods [28] and ZnO nanorods [29] have been reported in the literature. At the same time, PVP is present as the surface stabilizer, and its long polymeric chain structure will completely surround one or more Sb_2O_3 nuclei. What is more, we believe that PVP can selectively adsorb on the specific plane of Sb_2O_3 and control the growth of the one-dimensional nanowires with rectangular cross sections. On the basis of the above analysis, the reaction that occurred in the formation of the Sb_2O_3 crystal nucleus may be illustrated as follows:

$$4Sb + 3O_2 \xrightarrow[PVP,\ H_2O]{EDA} 2Sb_2O_3$$

In order to clarify the formation of the rectangular cross sections, SEM images of the time-depended shape evolution of the as-synthesized Sb_2O_3 nanowires with rectangular cross sections at different intervals are shown in Figure 5. As shown in Figure 5a, one can clearly see that the faceted Sb_2O_3 nanoparticles were formed at first (as the cycle indicates), which acted as the nucleus for further growth of nanorods. As shown in Figure 5b and c, the Sb_2O_3 faceted nucleus grew to form 1D Sb_2O_3 nanorods with rectangular faces as the time increased to 60 min, and the arrows in Figure 5c indicate that the sites the growth took place at were at the tips of the nanorods with rectangular faces. Finally, as shown in Figure 5d, the Sb_2O_3 nanorods further grew into uniform Sb_2O_3 nanowires with rectangular cross sections along the growth directions, extending their lengths. What is more, as shown above, PVP is present as the surface stabilizer, and selectively adsorbs on the specific plane of Sb_2O_3 and controls the growth of the 1D nanowires with rectangular cross sections in the overall growth process. It is believed that the products grow through a typical dissolution−recrystallization process followed by the Ostwald ripening mechanism, in which the growth progress is controlled by mass transport and by surface equilibrium of addition and removal

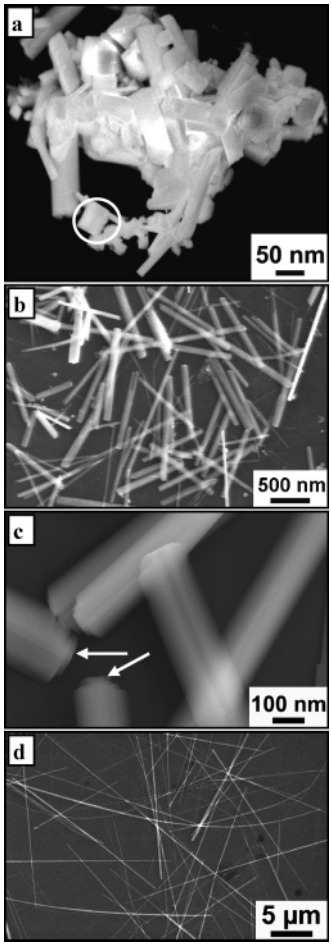

Figure 5. SEM images of the time-depended size and shape evolution of the as-synthesized Sb_2O_3 nanowires with rectangular cross sections at different intervals: (a) 10, (b and c) 60, and (d) 300 min. The cycle in part a indicates the formation of the facet nanoparticles, and the arrows in part c indicate the growth sites of the Sb_2O_3 nanorods with rectangular cross sections.

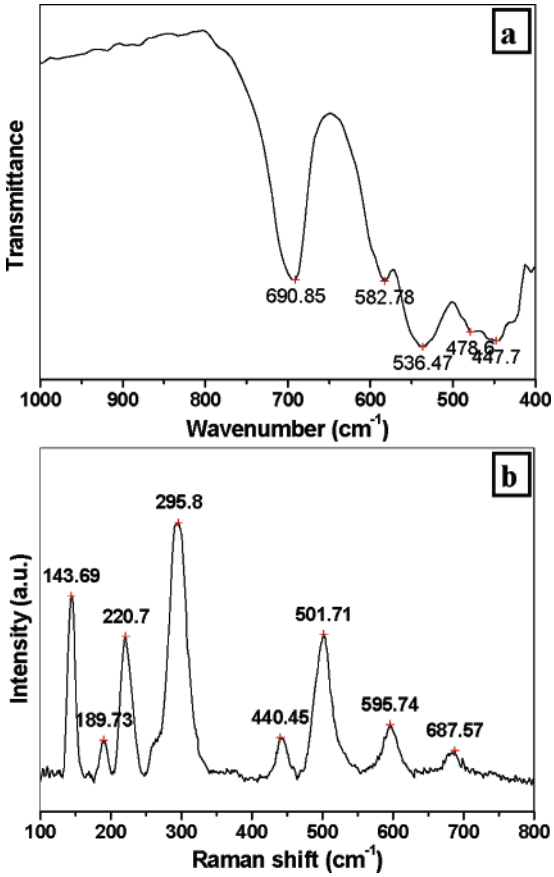

Figure 6. (a) Room temperature FTIR and (b) Raman spectra of the as-synthesized Sb_2O_3 nanowires.

of individual monomers. However, the understanding of the exact growth mechanism is still in progress.

The vibration spectra of the as-synthesized products were further investigated by room temperature FTIR and Raman spectra as shown in Figure 6. Antimony trioxide used in this experiment shows signals in the room temperature FTIR spectrum (Figure 6a) at 447.7, 478.6, 536.47, 582.78, and 690.85 cm^{-1}. A comparison with the IR data of Cody's work[30] reveals that the bands observed at 455, 488, 540, 585, and 740 cm^{-1} are normally IR-active modes, close to our results. In addition, the high crystallinity of the sample may lead to some strengthening of the spectroscopic selection rule for different bands. The signal registered at 690.85 cm^{-1} is absent in bulk Sb_2O_3; however, this band is normally a Raman-active mode. What is more, the large Sb_2O_3 band at 740 cm^{-1} is missing in our products, which may be overlaid by the 690.85 cm^{-1} band because the latter band is very strong in the pattern. Furthermore, no other bands are observed at the positions expected for Sb_2O_3.

The two common forms of Sb_2O_3 are the cubic phase senarmontite and the orthorhombic phase valentinite.[31] Senarmontite (cubic Sb_2O_3) crystallizes in the face-centered cubic lattice of the space group $F3dm$-O_h^7, with a unit cell of dimension 1.114 nm, which is built of discrete Sb_4O_6 molecules and is isomorphous to arsenite (As_4O_6) in which the M_4O_6 unit also occurs and which contains eight molecules in the face-centered unit cell and two molecules in the primitive cell. Valentinite (orthorhombic Sb_2O_3) crystallizes in the orthorhombic space group D_{2h}^{10} with the unit-cell dimensions of $a = 0.492$ nm, $b = 1.246$ nm, and $c = 0.542$ nm, which is built up by infinite polymeric Sb−O−Sb chains running along the c axis with Sb−O distances of 0.200 nm.[30,31] Therefore, the Raman spectrum in the internal mode region (400−800 cm^{-1}) of orthorhombic Sb_2O_3 is mainly dependent on the spectral features of polymeric Sb−O chains. The lattice mode region below 400 cm^{-1}, however, is controlled by the crystal space group and unit cell coupling.[31] Thus, all signals below 400 cm^{-1} belong to the external lattice mode regime, while those above 400 cm^{-1} belong to the internal vibrations. Antimony trioxide used in this experiment shows signals in the room temperature Raman spectrum (Figure 6b) at 143.69, 189.73, 220.7, 295.8, 440.45, 501.71, 595.74, and 687.57 cm^{-1}, which fit well with the data of Cody et al. (141, 189, 219, 295, 500, 596, and 690 cm^{-1})[30] and should be attributed to orthorhombic phase valentinite. The assignment of the signals of cubic Sb_2O_3 has been carried out following Beattie and co-workers;[31] unfortunately, for orthorhombic Sb_2O_3 the signals remain unassigned in the literature. In addition, we also have characterized the FTIR and Raman spectra of the calcined products, and found that the FTIR and Raman patterns of the calcined products are almost the same as those of the uncalcined products, suggesting that the well-crystallized Sb_2O_3 nanowires with rectangular cross sections obtained from the solution are free from antimony-hydroxo or antimony-aqua complex species.

The band gap of the bulk Sb_2O_3 crystal is 3.30 eV, which was determined by the UV−Vis−NIR transmission spectrum in the 1970s,[32−34] and little additional work has been presented in the literature since then. Herein, an optical absorption experiment was carried out to elucidate information on the band

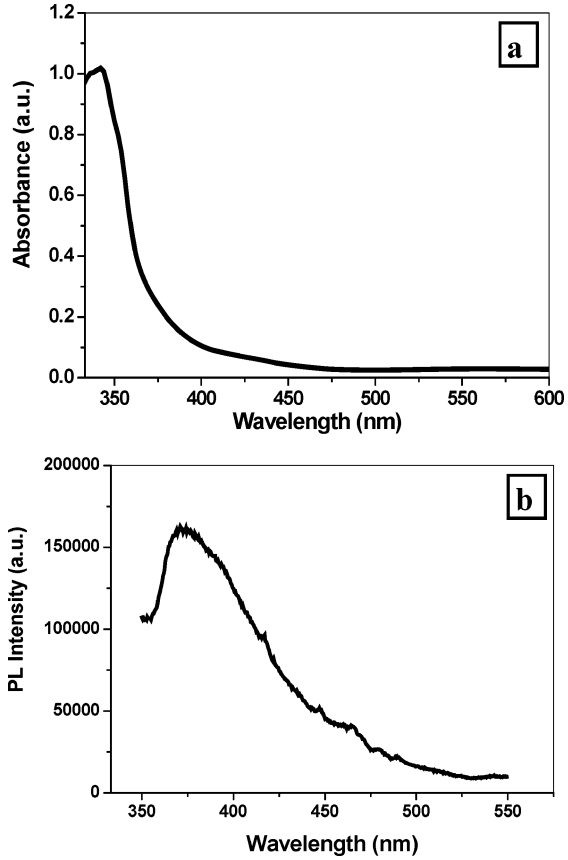

Figure 7. (a) Room temperature UV−visible absorption and (b) photoluminescence spectra obtained from the as-synthesized Sb_2O_3 nanowires; the λ_{ex} is at 325 nm.

gap energy, which is one of the most important electronic parameters for semiconductor nanomaterials. Shown in Figure 7a is a typical UV−visible absorption spectrum of the Sb_2O_3 nanowires with rectangular cross sections. The onset of the spectrum recorded from the nanowires with a rectangular cross section sample is about 376 nm, thus the band gap of the Sb_2O_3 nanowires may be estimated at 3.3 eV by using the same formula determined by other groups.[35,36] The profile between 376 and 450 nm is probably partially due to the scattering. Due to the fact that nanowires with rectangular cross sections are about 80−100 nm in width and 60−80 nm in thickness, we do not expect the corresponding E_g is very different from that of bulk materials. The experimentally determined E_g value of our Sb_2O_3 nanowires with rectangular cross sections is near that of ZnO, which suggests that Sb_2O_3 nanowires with rectangular cross sections may be very promising for applications in optical and electronic nanodevices.

The most unique feature of the as-synthesized Sb_2O_3 nanowires with rectangular cross sections has been found by measuring the photoluminescence. Figure 7b shows the room temperature emission spectrum obtained with an excited wavelength of 325 nm, in which a relatively strong emission band at about 374 nm is observed, indicating Sb_2O_3 nanowires with an optical band gap $E_g = 3.3$ eV. We have also examined the emission spectra of the nanowires excited under different wavelengths, such as 290, 310, and 340 nm (see Figure S1, Supporting Information). It can be seen that the emission peak position of the products at 374 nm remained almost unchanged under different excitation wavelengths, showing intrinsic properties of the nanowires themselves. It is worth noting that pure bulk antimony and bulk phase Sb_2O_3 powder has a negligible or no luminescence signal under the same excitation conditions. As seen from the characterization results, such as the XRD, SAED, and EDX, the products are highly pure Sb_2O_3 nanowires, thus we expect the photoluminescence spectrum represents the true photoluminescence behavior of the Sb_2O_3. To the best of our knowledge, this band edge emission is reported for the first time for Sb_2O_3.

Bulk phase Sb_2O_3 is an indirect-gap semiconductor with very low emission efficiency. It is believed that in the bulk crystal of indirect-gap materials, the electron−hole combination is possible only through phonon emission or absorption for the wave vector compensation. However, it is well-known that photoluminescence has been observed for indirect gap semiconductors such as Si and Ge, when their sizes fell into the nanoscale. Studies on this photoluminescence reveal quantum-confinement-induced indirect-to-direct gap conversion in the nanostructures, strongly suggesting the importance of the low-dimensional effect in the luminescence process. On account of the nanoscale sizes of the rectangular cross sections of as-synthesized Sb_2O_3 nanowires, the observed relatively strong UV emission band at about 374 nm may be associated with the low-dimensional effect on the band gap.[37] As a result, we believe that the emissions observed may be attributed to the band−band transition. Furthermore, as seen from the results of SEM, TEM, SAED, HRTEM, FTIR, and Raman, the as-synthesized products are uniform, single-crystalline, well-faceted orthorhombic nanowires, thus we expected that the oxygen vacancies or defects for the nanowires are negligible; as a result, the blue emission of the nanowires, which is commonly seen in ZnO 1D nanostructures due to the localized states induced by the presence of oxygen vacancies or defects in the nanostructure, was not observed in the photoluminescence emission spectrum. In addition, the unique rectangular cross section possibly has a shape effect on the photoluminescence properties of nanowires. Indeed, some similar novel luminescence phenomena also have been observed in other metal oxide semiconductor nanostructures such as NiO[38] and WO_3.[39] Actually, there is a lack of investigations on luminescence in the Sb_2O_3 systems so that the origin and the mechanism of the emission requires further investigations.

4. Conclusions

Uniform Sb_2O_3 nanowires with rectangular cross sections were synthesized by direct air oxidation of bulk metal antimony (Sb) in a mixed solution made of ethylenediamine (EDA) and deionized water (DIW), without common antimony salts used in the experiment. Comprehensive structural investigations including XRD, SAED, and HREM show that the nanowires with rectangular cross sections are pure orthorhombic phase Sb_2O_3. The nanowires with rectangular cross sections grow along the [001] direction. The growth mechanism of the nanowires was investigated based on the SEM observations. The UV−visible absorption spectrum reveals that the nanowires with rectangular cross sections are semiconductors with a band gap of about 3.3 eV, near ZnO; the discovery of a completely unexpected luminescence emission deserves additional investigation, which suggests that Sb_2O_3 nanowires with rectangular cross sections may be very promising new members in the family of functional semiconductor materials and are expected to be used in the manufacture of advanced nanodevices. By the suitable choice of source and synthetic parameters, it is reasonable to expect that the present study could be extended to the synthesis of other 1D metal oxide semiconductor nanostructures.

Acknowledgment. The current investigations are financially supported by the National Natural Science Foundation of China (60572031, 60372009, 20301015), the nanobiomedical and device applications of CAS (No: Kjcx-sw-h12), and the 973 project of China (2002CB713802). The authors wish to express their appreciation and thanks to Professor Qing Chen in Peking University, Beijing, China for her helpful suggestions.

Note Added after ASAP Publication. This paper was published ASAP on August 23, 2006. A typographical error was corrected in the third paragraph of the Results and Discussion. The revised paper was reposted on August 31, 2006.

Supporting Information Available: The PL spectra of the as-synthesized Sb_2O_3 nanowires excited at various wavelengths. This material is available free of charge via the Internet at http://pubs.acs.org.

References and Notes

(1) Huang, M. H.; Mao, S.; Feick, H.; Yan, H. Q.; Wu, Y. Y.; Kind, H.; Weber, E.; Russo, R.; Yang, P. D. *Science* **2001**, *292*, 1897.

(2) Cui, Y.; Wei, Q. Q.; Park, H. K.; Lieber, C. M. *Science* **2001**, *293*, 1289.

(3) Pan, Z. W.; Dai, Z. R.; Wang, Z. L. *Science* **2001**, *291*, 1947.

(4) Kind, H.; Yan, H. Q.; Messer, B.; Law, M.; Yang, P. D. *Adv. Mater.* **2002**, *14*, 158.

(5) Melosh, N. A.; Boukai, A.; Diana, F.; Gerardot, B.; Badolato, A.; Petroff, P. M.; Heath, J. R. *Science* **2003**, *300*, 112.

(6) Duan, X. F.; Huang, Y.; Agarwal, R.; Lieber, C. M. *Nature* **2003**, *421*, 241.

(7) Kong, X. Y.; Wang, Z. L. *Solid State Commun.* **2003**, *128*, 1.

(8) Wang, Z. L. *Annu. Rev. Phys. Chem.* **2004**, *55*, 159.

(9) Zhang, J.; Jiang, F. H.; Zhang, L. D. *Phys. Lett. A* **2004**, *322*, 363.

(10) Yang, R. S.; Wang, Z. L. *J. Am. Chem. Soc.* **2006**, *128*, 1466.

(11) Chand, N.; Verma, S. *J. Fire Sci.* **1991**, *9*, 251.

(12) Sato, H.; Kondo, K.; Tsuge, S.; Ohtani, H.; Sato, N. *Polym. Degrad. Stab.* **1998**, *62*, 41.

(13) Longerey, M.; Cuesta, J. M.; Gaudon, P.; Crespy, A. *Polym. Degrad. Stab.* **1999**, *64*, 489.

(14) Spengler, J.; Anderle, F.; Bosch, E.; Grasselli, R. K.; Pillep, B.; Behrens, P.; Lapina, O. B.; Shubin, A. A.; Eberle, H. J.; Knozinger, H. *J. Phys. Chem. B* **2001**, *105*, 10772.

(15) Liu, H. C.; Imoto, H.; Shido, T.; Iwasawa, Y. *J. Catal.* **2001**, *200*, 69.

(16) Duh, B. *Polymer* **2002**, *43*, 3147.

(17) Liu, H. H.; Iwasawa, Y. *J. Phys. Chem. B* **2002**, *106*, 2319.

(18) Guo, L.; Wu, Z. H.; Liu, T.; Wang, W. D.; Zhu, H. S. *Chem. Phys. Lett.* **2000**, *318*, 49.

(19) Chen, X. Y.; Wang, X.; An, C. H.; Liu, J. W.; Qian, Y. T. *Mater. Res. Bull.* **2005**, *40*, 469.

(20) Friedrichs, S.; Meyer, R. R.; Sloan, J.; Kirkland, A. I.; Hutchison, J. L.; Green, M. L. *Chem. Commun.* **2001**, 929.

(21) Ye, C. H.; Meng, G. W.; Zhang, L. D.; Wang, G. Z.; Wang, Y. H. *Chem. Phys. Lett.* **2002**, *363*, 34.

(22) Zhang, Y. X.; Li, G. H.; Zhang, J.; Zhang, L. D. *Nanotechnology* **2004**, *15*, 762.

(23) Sendor, D.; Weirich, T.; Simon, U. *Chem. Commun.* **2005**, 5790.

(24) Xiong, Q. H.; Wang, J. G.; Reese, O.; Voon, L. C. L. Y.; Eklund, P. C. *Nano Lett.* **2004**, *4*, 1991.

(25) Zhang, D.-F.; Sun, L.-D.; Yin, J.-L.; Yan, C.-H.; Wang, R.-M. *J. Phys. Chem. B* **2005**, *109*, 8786.

(26) Wen, X.; Fang, Y.; Pang, Q.; Yang, C.; Wang, J.; Ge, W.; Wong, K. S.; Yang, S. *J. Phys. Chem. B* **2005**, *109*, 15303.

(27) Guiton, B. S.; Gu, Q.; Prieto, A. L.; Gudiksen, M. S.; Park, H. *J. Am. Chem. Soc.* **2005**, *127*, 498.

(28) Sampanthar, J. T.; Zeng, H. C. *J. Am. Chem. Soc.* **2002**, *124*, 6668.

(29) Pal, U.; Santiago, P. *J. Phys. Chem. B* **2005**, *109*, 15317.

(30) Cody, C. A.; Dicarlo, L.; Darlington, R. K. *Inorg. Chem.* **1979**, *18*, 2.

(31) Mestl, G.; Ruiz, P.; Delmon, B.; Knozinger, H. *J. Phys. Chem.* **1994**, 11276.

(32) Tigau, N.; Ciupina, V.; Prodan, G.; Rusu, G. I.; Vasile, E. *J Cryst. Growth* **2004**, *269*, 392.

(33) Wood, C.; Van Pelt, B.; Dwight, A. *Phys. Status Solidi B* **1972**, *54*, 701.

(34) B. Wolffing, Z. Hurych, *Phys. Status Solidi A* **1973**, *16*, 161.

(35) Zheng, X. W.; Xie, Y.; Zhu, L. Y.; Jiang, X. C.; Jia, Y. B.; Song, W. H.; Sun, Y. P. *Inorg. Chem.* **2002**, *41*, 455.

(36) Yu, Y.; Wang, R. H.; Chen, Q.; Peng, L. M. *J. Phys. Chem. B* **2005**, *109*, 23312.

(37) Pan, A. L.; Liu, D.; Liu, R. B.; Wang, F. F.; Zhu, X.; Zou, B. S. *Small* **2005**, *1*, 980.

(38) Wu, Z. Y.; Liu, C. M.; Guo, L.; Hu, R.; Abbas, M. I.; Hu, T. D.; Xu, H. B. *J. Phys. Chem. B* **2005**, *109*, 2512.

(39) Feng, M.; Pan, A. L.; Zhang, H. R.; Li, Z. A.; Liu, F.; Liu, H. W.; Shi, D. X.; Zou, B. S.; Gao, H. J. *Appl. Phys. Lett.* **2005**, *86*, 141901.